ACS APPLIED MATERIALS & INTERFACES

Research Article

www.acsami.org

Influence of Porphyrinic Structure on Electron Transfer Processes at the Electrolyte/Dye/TiO_2 Interface in PSSCs: a Comparison between meso Push−Pull and β-Pyrrolic Architectures

Gabriele Di Carlo,*[,†] Stefano Caramori,*[,‡] Vanira Trifiletti,[§] Roberto Giannuzzi,[§] Luisa De Marco,[§] Maddalena Pizzotti,[†] Alessio Orbelli Biroli,[⊥] Francesca Tessore,[†] Roberto Argazzi,[#] and Carlo A. Bignozzi[‡]

[†]Department of Chemistry, University of Milan, INSTM Research Unit, Via C. Golgi 19, 20133 Milano, Italy

[‡]Department of Chemistry and Pharmaceutical Sciences and [#]ISOF/CNR c/o Department of Chemistry and Pharmaceutical Sciences, University of Ferrara, Via Fossato di Mortara 17, 44121 Ferrara, Italy

[§]CBN, Center for Biomolecular Nanotechnologies, Fondazione Istituto Italiano di Tecnologia Energy Platform Via Barsanti, 73010 Arnesano (Lecce), Italy

[⊥] Istituto di Scienze e Tecnologie Molecolari del CNR (CNR-ISTM), Via C. Golgi 19, 20133 Milano (Italy)

Supporting Information

ABSTRACT: Time-resolved photophysical and photoelectrochemical investigations have been carried out to compare the electron transfer dynamics of a 2-β-substituted tetraarylporphyrinic dye (ZnB) and a 5,15-meso-disubstituted diarylporphyrinic one (ZnM) at the electrolyte/dye/TiO_2 interface in PSSCs. Although the meso push−pull structural arrangement has shown, up to now, to have the best performing architecture for solar cell applications, we have obtained superior energy conversion efficiencies for ZnB (6.1%) rather than for ZnM (3.9%), by using the I^-/I_3^--based electrolyte. To gain deeper insights about these unexpected results, we have investigated whether the intrinsic structural features of the two different porphyrinic dyes can play a key role on electron transfer processes occurring at the dye-sensitized TiO_2 interface. We have found that charge injection yields into TiO_2 are quite similar for both dyes and that the regeneration efficiencies by I^-, are also comparable and in the range of 75−85%. Moreover, besides injection quantum yields above 80%, identical dye loading, for both ZnB and ZnM, has been evidenced by spectrophotometric measurements on transparent thin TiO_2 layers after the same adsorption period. Conversely, major differences have emerged by DC and AC (electrochemical impedance spectroscopy) photoelectrochemical investigations, pointing out a slower charge recombination rate when ZnB is adsorbed on TiO_2. This may result from its more sterically hindered macrocyclic core which, besides guaranteeing a decrease of π-staking aggregation of the dye, promotes a superior shielding of the TiO_2 surface against charge recombination involving oxidized species of the electrolyte.

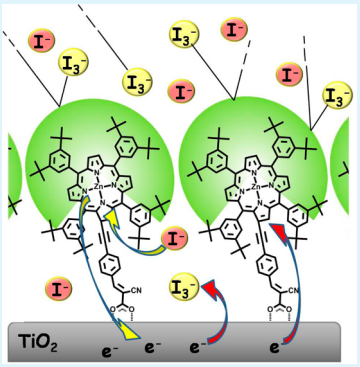

KEYWORDS: *porphyrins, solar cell, regeneration kinetics, recombination, interfacial dynamics*

INTRODUCTION

In the last two decades, porphyrinic molecules have emerged as promising sensitizers for dye-sensitized solar cells (DSSC). To date, numerous metal porphyrins have been investigated for this purpose by virtue of their intrinsic advantages such as high chemical and photochemical stability and their strong electronic absorption and emission bands up to the near-infrared region. The electrochemical[1,2] and light-harvesting properties[3−7] of such molecules are easily tunable acting, with specific chemical functionalizations, either on four meso or eight β-pyrrolic positions.

Typically 5,15 meso disubstituted push−pull metal porphyrins are featured by a low HOMO−LUMO energy gap, by significant charge separation character and, in particular, by efficient electron transfer processes from the donor to the acceptor group through the push−pull system.[8,9] For this reason, such a series of metal porphyrins has been largely investigated as dyes for solar cell applications. As a consequence, DSSC devices have been, so far, properly optimized for these type of sensitizers. For instance, 5,15-meso push−pull Zn^{II} porphyrinates, well engineered with bulky alkyl chain substituents, have reached the best power conversion efficiencies (exceeding 12%), hitherto obtained in a Porphyrin Sensitized Solar Cell (PSSC) device using cobalt-based mediators.[10−12]

Despite their relevant photoelectrochemical advantages,[3] the asymmetric 5,15 meso disubstituted push−pull metal porphyrins are very hard to obtain by an effective synthetic route and,

Received: May 20, 2014
Accepted: August 4, 2014
Published: August 4, 2014

in particular, the multistep synthetic procedures drastically reduce the overall yields.[4,5,13,14] Furthermore, without additional sterically hindered substituents, their quite planar structures promote π-staking aggregation which may be detrimental for the efficiency of DSSC devices. All these reasons result in a dramatic reduction of the intrinsic benefits to the replacement of traditional dyes based on rare metals (Ru, Os) by this kind of porphyrinic sensitizers. A synthetically attractive alternative to the meso push−pull porphyrinic dyes could be the β-substituted metal porphyrins, due to the symmetric tetraaryl-porphyrinic core which can be easily obtained with excellent yield via one-pot reaction between pyrrole and appropriate aryl-aldehydes.[15,16] Moreover, the purification processes of such bulky porphyrinic dyes are significantly improved because of their enhanced solubility.

However, nowadays, few DSSC devices were investigated and optimized involving β-substituted tetraaryl Zn^{II} porphyrinates as dyes,[15,17−24] although remarkable light-conversion efficiencies of up to 7.1% have been reached with relatively simple molecular architectures.[7]

Recently, with the aim to focus further attention on such a promising class of green and stable porphyrinic dyes, a microwave-assisted synthetic approach was exploited, by some of us,[17] to successfully obtain a series of β-substituted Zn^{II} porphyrinates in a few steps. These dyes were characterized by relatively broad photoaction spectra in the 350−650 nm range, with maximum monochromatic conversions exceeding 60%. Surprisingly, both β mono- and disubstituted push−pull Zn^{II} porphyrins, when used as dyes in DSSCs based on iodide/iodine electrolyte, resulted in either similar or superior efficiencies when compared with related homologues arranged in a meso disubstituted push−pull geometry. Moreover, density functional theory (DFT) computational investigations suggested that the increased energy conversion efficiency arising from β substitution of the porphyrinic ring could be probably ascribed to more facile charge injection into the TiO_2 acceptor states.[17] Hence, starting from such assumption, with the aim to gain deeper insights about injection, regeneration and recombination, the dynamics of electron transfer processes, which occur at the interface of electrolyte/dye/TiO_2, are thoroughly investigated here.

Previous photophysical and photoelectrochemical investigations of β-substituted porphyrins absorbed on TiO_2 film have revealed improved charge transfer when compared with meso substituted porphyrin carboxylic acids[21] and higher injection rates with respect to Ru-based dye, N719.[25] Besides, a comparative study about electron injection and recombination kinetics, based on time-resolved optical and electrical probes focused on variously substituted porphyrinic dyes, pointed out that the critical factor in determining the injection efficiency was not the linker substitution position.[22]

To date, to the best of our knowledge, no comparative time-resolved photophysical investigation has been ever carried out between 2-β-substituted tetraarylporphyrinic dyes and their 5,15-meso disubstituted push−pull diarylporphyrinic counterparts. These latter dyes, being featured by a donor−π−acceptor (D−π−A) architecture[14] that introduces a strong charge transfer character of the excited state, are usually considered to be the best-performing dyes when compared to both β and meso monosubstituted metal porphyrins where the porphyrinic core itself acts as electron donor because it lacks the push−pull arrangement.[3,6,21,22]

However, the charge injection kinetic is not the only critical factor in determining the efficiency of a DSSC device. Charge recombination processes between sensitized TiO_2 nanocrystalline electrode and the dye cation or the oxidized electrolyte (I_3^-) (Figure 1), usually occurring on a much longer time scale

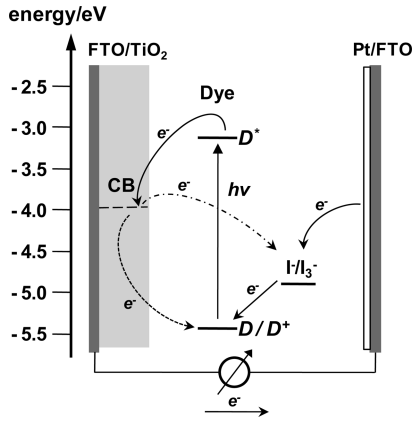

Figure 1. Schematic illustration of electron transfer processes: injection (solid arrow) from photoxcited dye into conduction band (CB), recombination from CB to the dye cation (dot arrow) or to the redox mediator I_3^- (dash-dot arrow).

(ns−ms) with respect to injection process, are indeed of paramount importance in determining the DSSC performance. Furthermore, such recombination events strongly depend on the molecular architecture of the dye, because its adsorption geometry may influence the interactions between TiO_2 surface and redox mediators, by determining the coverage and the passivation of the TiO_2 surface against the recombination involving the approach of I_3^- to the exposed photoanodic surface.[18,26] To prevent such an undesired interaction, two approaches were previously reported. The first concerning the insertion of long alkoxyl chains to protect the porphyrinic core was exploited to retard both charge recombination and effectively decrease dye aggregation.[5] A further attractive approach, which involved the use of fatty acids as coadsorbent of an organic sensitizer, allowed to obtain efficient recombination barriers by limiting the access of I_3^- to the photoanode surface.[27]

In this work, we comparatively investigate various processes of charge transfer and charge recombination of two porphyrinic dyes, ZnB and ZnM, featured by structural arrangements based on 2-β monosubstituted and 5,15-meso push−pull disubstituted Zn^{II}-porphyrinates respectively (Chart 1). Furthermore, photovoltaic characteristics of DSSCs based on such porphyrinic dyes are studied using I^-/I_3^- mediator to properly compare the obtained data with those previously reported by some of us.[17] Time-resolved photophysical studies, photoelectrochemical investigations and, in particular, Electrochemical Impedance Spectroscopy (EIS) were combined with the aim of characterizing the fundamentals of the interfacial charge separation and collection processes on porphyrin-sensitized TiO_2 surface. Such an in-depth investigation was carried out with the specific purpose of defining the fundamental aspects for disproving the "paradigm" for which, in case of porphyrin sensitized solar cells, the best performing architecture of dyes requires a meso disubstituted push−pull arrangement.[3] In fact, some of us, in a comparative study between the β-substituted and meso disubstituted push−pull Zn^{II}-porphyrinates, used as sensitizers

Chart 1. Structures of the Two Zn^{II}-Porphyrinates Investigated in This Work

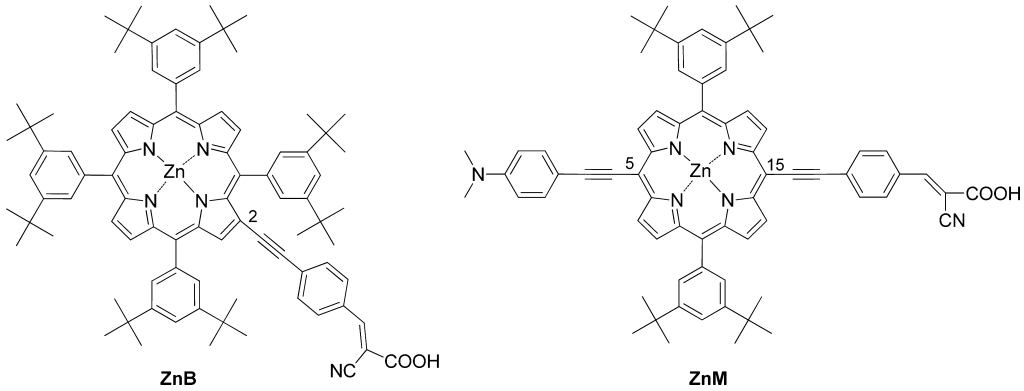

in properly engineered DSSC devices,[17] have recently reported higher energy conversion efficiencies in case of ZnB rather than ZnM. It follows that the information reached in this work may be helpful in guiding the development of new efficient β-substituted porphyrinic dyes, which thanks to their relatively straightforward and effective synthetic pathway, may be the basis of inexpensive DSSCs with excellent performances.

EXPERIMENTAL SECTION

Materials. All reagents and solvents used in the synthesis were purchased by Sigma-Aldrich and used as received, except Et_3N, Et_2NH (freshly distilled over KOH) and THF (freshly distilled from Na/benzophenone under nitrogen atmosphere). Silica gel for gravimetric chromatography (Geduran Si 60, 63−200 μm) and for flash chromatography (Geduran Si 60, 40−63 μm) were purchased by Merck. Glassware was flame-dried under vacuum before use when necessary. Microwave assisted reactions were performed using a Milestone MicroSYNTH instrument.

Transparent semiconductor thin films on FTO substrates, intended for optical spectroscopy, were prepared by blade casting a nanocrystalline paste of either TiO_2 (Dyesol DSL18NR-T) or ZrO_2, followed by drying and sintering at 450 °C for 45 min. The 15% w/w ZrO_2 aqueous paste was obtained by the slow acidic hydrolysis of Zr(IV) tetra-iso-propoxide,[14] followed by hydrothermal nucleation and growth at 220 °C for 12 h and final addition of 40% w/w (with respect to ZrO_2) Carbowax 20000 as a sintering agent.

Synthesis of Porphyrinic Dyes. ZnB and ZnM were prepared as reported elsewhere.[17] The syntheses of tetraaryl Zn^{II}-porphyrinates substituted in the β-pyrrolic position involved an optimized synthetic route based on a microwave-enhanced Sonogashira coupling approach. First, the symmetric tetraaryl-porphyrinic core was effectively obtained by one-step cyclization between 3,5-Di-*tert*-butylbenzaldehyde and pyrrole followed by the metalation step with Zn^{II}. Subsequently, the pyrrolic functionalization with NBS, followed by Sonogashira coupling reaction and the Knoevenagel condensation, have finally allowed to obtain the desired dye ZnB with good yield. On the other hand, the synthesis of ZnM with meso architecture was performed by a classical approach requiring a multistep procedure. The starting diarylporphyrinic core was prepared via dipyrromethane synthetic pathway in a two-step process. The iodination of the meso positions was followed by the Zn^{II} metalation step and the thermal Sonogashira coupling reaction allowed to link either donor- and acceptor-moiety to the porphyrin core. The ZnM was finally obtained by a Knoevenagel condensation. Such a standard synthetic route is featured by significantly lower overall yield with respect to the ZnB synthetic procedure.

Preparation of DSSCs. Fluorine-doped tin oxide (FTO, 10 Ω/Sq, provided by Solaronix S.A.) were cleaned in a detergent solution for 15 min and in EtOH for 30 min using an ultrasonic bath, and finally rinsed with absolute EtOH. FTO plates were then treated with a 40 mM aqueous solution of $TiCl_4$ for 30 min at 70 °C and then rinsed with EtOH. The photoelectrodes, obtained by doctor blading, were composed of a double layer consisting of anatase nanoparticles of different dimensions: Dyesol 18NR-T, which gave transparent 9.0-μm TiO_2 films, and Solaronix D/SP, which was used as active/opaque overlayer with thickness of 7-μm, resulting in a total active layer of 16-μm. The coated films were dried at 125 °C for 5 min, after each layer deposition, and then thermally treated 450 °C for 30 min. The sintered layer was treated again with 40 mM aqueous $TiCl_4$ (70 °C for 30 min), rinsed with EtOH and heated at 450 °C for 30 min. After cooling to 80 °C the TiO_2 coated plate was immersed into a 0.2 mM solution of the dye in EtOH/THF 9:1 containing chenodeoxycholic acid (CDCA, 0.2 mM) for 2 h at room temperature in the dark. The thickness of the layer was measured by means of a profilometer (Tencor Alpha-Step 500 Surface Profiler). The counter electrode was prepared according to the following procedure: first, a 1.8 mm hole was made in a FTO plate using diamond drill bits, then, the electrode was cleaned for 30 min using a solution of EtOH and HCl and finally with acetone for 15 min, in an ultrasonic bath. After heating at 450 °C for 30 min, 200 μL of H_2PtCl_6 (5×10^{-3} M solution in EtOH) were dropped on the cooled substrates, followed by firing at 530 °C for 1h. The dyed TiO_2 photoelectrode and the counter electrode were assembled by heating a gasket made of a thermoplastic ionomer-class resin (Surlyn 50-μm thickness). The electrolyte Z959 (1.0 M 1,3-dimethylimidazolium iodide, 0.03 M I_2, 0.10 M guanidinium thiocyanate, and 0.50 M 4-*tert*-butylpyridine in acetonitrile/valeronitrile, 85:15) was introduced inside the cell by vacuum backfilling. Finally, the hole was sealed with adhesive tape and a reflective foil at the back side of the counter electrode was applied to reflect unabsorbed light back to the photoanode.

Photoelectrochemical Measurements. Photovoltaic $J-V$ curves were obtained using a Newport AM 1.5 Solar Simulator (Model 91160A equipped with a 300W xenon arc lamp) as a light source and a Keithley unit (model 2400 Source Meter). The light intensity was calibrated to 100 mW cm^{-2} using a Si solar cell as a reference. The measurements were carried out using a black metal mask of 0.16 cm^2.

The incident photon-to-current conversion efficiency (IPCE) measurements were carried out by a DC method with a computerized setup consisting of a xenon arc lamp (140 W, Newport, 67005) coupled to a monochromator (Cornerstone 260 Oriel 74125). Light intensity was measured by a calibrated UV silicon photodetector (Oriel 71675) and the short circuit currents of the DSSCs were measured by using a dual channel optical power/energy meter (Newport 2936-C).

Electrochemical impedance spectroscopy (EIS) was performed with an AUTOLAB PGSTAT 302N (Eco Chemie B.V.) in a frequency range between 300 kHz and 30 mHz. The impedance measurements were carried out at different voltage biases in dark condition and under 1 sun illumination. The resulting impedance spectra were fitted with ZView software (Scribner Associates).

Photophysical Measurements. Stationary UV−Vis spectroscopy was performed with an Agilent Cary 300 Spectrophotometer.

Stationary emission spectroscopy was carried out with an Edinburgh Instruments FLS 920 Spectrofluorimeter equipped with a double emission monochromator. Spectral bandwidths of 2 nm were usually employed and the S/N ratio was optimized by summing 10 subsequent scans with 1 nm wavelength step. Spectra were corrected for the photomultiplier (R928P-Hamamatsu) response by using a factory built in calibration file. Excitation was into the Soret Band of the respective porphyrin sensitized solid thin films in the presence of 0.1 M Li^+ in order to reproduce the local ionic environment of the operational DSSC. Before each emission measurement, sensitized TiO_2 and ZrO_2 thin films were soaked in $CH_3CN/LiClO_4$ for 10 min, covered with a glass slide, and placed in a dedicated film holder equipped with a micrometric mechanical regulation stage. To attain a good reproducibility, before collecting the whole spectrum, we optimized the maximum emission intensity by manually acting on the micrometric stage in order to fine-tune the angle between the thin film, the excitation beam and the emitted light reaching the detector. Background subtracted spectra, corrected for the light harvesting efficiency at the excitation wavelength λ_{ex} ($LHE_{(\lambda ex)} = (1-10^{-A(\lambda ex)})$ were integrated and averaged over a batch of four formally identical films of each substrate type (TiO_2 and ZrO_2).

Emission lifetimes of the dyes in either diluted THF/EtOH solution or loaded onto the solid thin films were recorded with a PicoQuant Picoharp 300 Time-Correlated Single Photon Counting (TCSPC) apparatus, by exciting at 460 nm (essentially the excitation was into the respective Soret Band of the two dyes) with a nanoled driven by a PDL 800 B pulsing unit (10 MHz, FWHM < 700ps). The films supported on FTO glass were immersed in a 0.1 M $LiClO_4$ solution oriented at 45° with respect to the excitation pulse and a 550 nm cut off filter prevented scattered excitation light from reaching the phototube. The collected emission wavelength corresponded to the first emission maximum of the sensitizer, observed in steady state emission spectroscopy.

Emission decays were either deconvolved from the excitation profile or tail-fitted according to a monoexponential function, with $\chi^2 < 1.5$, by using the dedicated program Fluofit.

Transient absorption spectroscopy (TAS) was performed with a previously described apparatus,[28] by using the 532 nm harmonic of a nanosecond Nd:YAG laser (Continuum Surelite II). When performing TAS on transparent thin films, the excitation energy was reduced to few mJ/cm^2/pulse by defocusing with a plano concave lens. A 532 nm notch filter prevented laser light from reaching the photomultiplier, whereas a 420 nm cut off filter, placed in front of the white light probe beam prevented direct TiO_2 excitation. From 10 to 30 laser shots, at a frequency of 0.2 Hz were averaged to reach a good S/N ratio.

TAS experiment on semitransparent ZrO_2 films were performed according to the previously described procedure except that two notch filters were serially placed in front of the entrance slit of the monochromator and a neutral filter (50% T) was used to attenuate the probe beam before passing through the sample. This was necessary to increase the S/N ratio and to reduce as much as possible scattering interferences from the thin films. Because of the comparatively low optical transmission of the ZrO_2 substrates with respect to TiO_2 ones, single wavelength oscillographic traces were generally averaged over 30 laser shots and fitted with monoexponential functions. To further improve the S/N ratio the ΔA values for building the TAS were obtained from the clean fitting curves.

TAS measurements in the presence of iodide-based electron donor (0.6 M Allyl-Methyl Imidaziolium iodide (AMII) + 0.1 M LiI in CH_3CN) were performed by drawing the electrolyte by capillarity inside the chamber (ca. 6−8 μm) constituted by a glass slide pressed against the TiO_2 photoanode. Thus, the negligible optical path allowed to avoid interferences originated by excitation of I_3^- created and accumulated at the interface during repeated measurements.

Computational Studies. Ground-state equilibrium geometries of ZnM and ZnB, preoptimized at the semiempirical PM6 level, were computed at the DFT B3LYP level by using a LANL2DZ basis set. The resulting structures were grafted to a TiO_2 surface slab ($Ti_{64}O_{128}$) oriented along the (101) plane previously optimized at the Molecular Mechanics (MM)-Universal Force Field (UFF) level. In order to preserve the equilibrium geometry of the porphyrins, computed at a reasonably high level of accuracy, all the internal coordinates of the assembly (porphyrin + TiO_2 slab) were frozen, with the exception of the C−COO−Ti linkage between the chromophore and the surface which was further optimized at the MM-UFF level to obtain reasonable bond distances and angles.

Space filling visualization was achieved by scaling the Van Der Waals radii to either 150 or 200%, as customary with the Gaussview 5 program. All calculations were carried out with Gaussian 09 C2 by using a multiple core (2× Intel quad core I7 processors) 64 bit PC running under Linux.

RESULTS AND DISCUSSION

Quenching of the Excited State on TiO_2 and ZrO_2 Thin Films and Injection Quantum Yield Evaluation. Quenching of the emission is a relatively straightforward qualitative method to evaluate the dye ability to inject charge into the acceptor states of TiO_2, by comparison with a semiconductor where charge injection is forbidden for energetic reasons. Herein ZrO_2 was chosen as an inert substrate since its lower conduction band edge (ca. −2 V vs SCE) is energetically out of reach by the excited state of most dyes. Moreover, ZrO_2 can be obtained in reasonably transparent films, which reduce scattering interferences during emission measurements and its surface chemistry is similar to that of TiO_2, resulting in a comparable dye loading when working in the same adsorption conditions.

Because photoinduced charge injection is thermodynamically forbidden, the only deactivation pathways of the excited state of porphyrinic dyes adsorbed on ZrO_2 surface are the radiative and non radiative mechanisms analogous to those occurring in solution. Furthermore, bimolecular quenching mechanisms, for example, exciton annihilation and/or excimer formation, can be reduced by working with relatively optically diluted films (Figure 2).

In Figure 2 are summarized the spectral properties of the two investigated porphyrinic dyes: both are characterized by the typical absorption spectrum of the porphyrinic structure, an intense Soret B-bands centered around 450 nm and weaker Q bands in the near-infrared region. The ZnM dye exploits a strong dipole moment, thanks to its push−pull architecture, resulting in a rather intense Q-band featured by a low energy maximum at 670 nm, whereas the ZnB dye shows comparatively weaker Q bands in the 530−630 nm region, reminiscent of more conventional symmetric Zn^{II}-porphyrinates. The absorption spectra of both dyes, anchored to TiO_2 and ZrO_2 semiconductors, retain the number of the Soret and Q bands. Although the absorption bands of the dyes grafted to ZrO_2 and TiO_2 are slightly broader than the corresponding bands in solution, no significant wavelength shifts are displayed. The band broadening of a dye loaded on a semiconductor thin layer may be due to the scattering effect of the films and is more prominent on ZrO_2 films, which are considerably more opaque than the equivalent TiO_2 substrates, as shown by their higher background at $\lambda \geq 800$ nm where no significant dye absorption is present (Figure 2).

The emission spectra of the dyes in solution (Figure 2) are generally in good agreement with the emission spectra recorded on ZrO_2 films (see Figure S1 in the Supporting Information). ZnB retains on both solid thin films and solution the well-defined vibronic structure with two main bands at 628 and 676 nm which compare very well with the maxima observed in fluid solution, at 624 and 677 nm, respectively. In the case of ZnM, the emission maximum on ZrO_2 is slightly blue-shifted (0.018

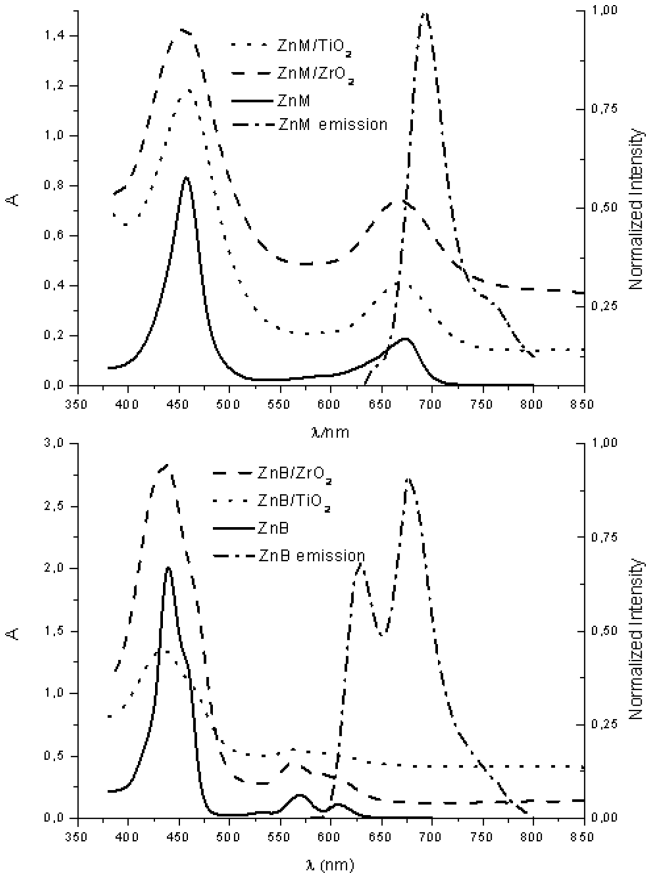

Figure 2. Overlayed absorption spectra of porphyrinic dyes (A) ZnM and (B) ZnB in EtOH/THF solution (solid line), loaded onto TiO_2 (dash) and ZrO_2 (dot) thin films. Normalized emission spectra in EtOH/THF solution (dash-dot).

eV) at 686 nm with respect to 693 nm found in solution. The emission of ZnM on solid thin film spans the same wavelength interval, from about 630 to 800 nm, but it is broader and the small vibronic shoulders at 642 and 757 nm are not observed. The broader spectrum is probably due to both scattering effects of ZrO_2 and to a partial aggregation of the meso architecture. The appearance of such a broad emission convolved with the 532 nm laser excitation was confirmed also during transient spectroscopy (see Figure S4B, D in the Supporting Information) experiments on ZrO_2, at very short delays (1−4 ns) after the laser pulse.

In case of the dyes loaded onto the TiO_2 surface, a strong quenching of the emission was revealed for both ZnM and ZnB, confirming that efficient photoinduced electron transfer occur from the dyes to the semiconductor surface (see Figure S2 in the Supporting Information).

In general the emission lifetime of dyes adsorbed on a semiconductor surface and in the presence of injection processes having a rate constant k_{inj} is given by

$$\tau = \frac{1}{k_r + k_{nr} + k_{inj}} \quad (1)$$

where k_r is the radiative rate constant, k_{nr} is the nonradiative rate constant and k_{inj} is the charge injection rate constant. Herein, k_{nr} includes both the rate constants for the Singlet to Triplet intersystem crossing (ISC) and for the Internal conversion (IC) vibrational relaxation to the ground state.

Given the similar surface chemistry and polarity of both TiO_2 and ZrO_2 surfaces, it is reasonable to assume that k_{nr} and k_r are identical for both dye-sensitized surfaces. As a result, neglecting bimolecular quenching mechanisms (or assuming that they are essentially the same on both TiO_2 and ZrO_2) k_{inj} can be obtained by determining the excited state lifetime on the two different semiconductors, through the straightforward relation

$$k_{inj} = \frac{1}{\tau_{TiO_2}} - \frac{1}{\tau_{ZrO_2}} \quad (2)$$

where τ_{TiO_2} and τ_{ZrO_2} are the emission lifetimes of dyes adsorbed on TiO_2 and ZrO_2 respectively. Emission lifetimes determined by time-correlated single photon counting (TCSPC) are reported in Table 1 and the relative emission decays are represented in Figure S2 in the Supporting Information. Monoexponential functions were used for both deconvolution and tailfitting with acceptable results ($\chi^2 < 1.5$). In solution, both dyes showed similar lifetimes, in the 1−2 ns time scale, consistent with singlet emissions. Once the dyes were adsorbed on both ZrO_2 and TiO_2 surfaces, the emission lifetimes were slightly shorter than those measured in solution, in the order of 0.9−1.2 ns. The lifetimes on TiO_2 are comparable or just marginally lower than those on ZrO_2 (1−0.95 ns), clearly contradicting the significant quenching observed in static emission experiments (see Figure S2 in the Supporting Information), suggesting that, on TiO_2 surface, most of the emission falls well within the excitation profile ($\tau_{TiO_2} < 300$ ps) of the TCSPC source. Reasonably, the observed relatively long-lived residual emission tail mostly comes from poorly surface coupled molecules, unable to perform electron transfer to the surface.

An evaluation of the excited state lifetime of the two porphyrinic dyes adsorbed on TiO_2, can be attempted by combining the stationary quenching results with the lifetimes on nanocrystalline ZrO_2 electrodes, where the excited state lifetime could be evaluated with a good degree of accuracy. The integrated emission spectra (see Figure S2 in the Supporting Information) once corrected for the LHE at the excitation wavelength (460 nm) are proportional to the respective emission quantum yields Φ_{em}, which refer on the radiative constant and on the lifetime according to the relation

$$\Phi_{em} = k_r \tau \quad (3)$$

Therefore, in the reasonable assumption that k_r is the same on both TiO_2 and ZrO_2 surfaces, it follows that

Table 1. Emission Lifetime Determined By TCSPC Upon 460 nm Excitation[a]

dye	τ (solution)[b] (ns)	τ (ZrO_2)[b] (ns)	τ (ZrO_2)[c] (ns)	τ (TiO_2)[b] (ns)	τ (TiO_2)[c] (ns)
ZnM	1.202 ± 0.001	0.922 ± 0.012	0.991 ± 0.018	0.965 ± 0.011	1.040 ± 0.011
ZnB	1.792 ± 0.006	1.116 ± 0.022	1.173 ± 0.026		0.954 ± 0.030

[a]Lifetimes are reported with their confidence intervals extracted from the fitting. [b]Deconvolution. [c]Tailfit.

$$\frac{I_{TiO_2}}{I_{ZrO_2}} = \frac{\Phi_{TiO_2}}{\Phi_{ZrO_2}} = \frac{\tau_{TiO_2}}{\tau_{ZrO_2}} \quad (4)$$

and

$$\tau_{TiO_2} = \frac{I_{TiO_2}}{I_{ZrO_2}} \tau_{ZrO_2} \quad (5)$$

Equation 5 yields the excited state lifetimes on TiO2 surface, equal to 95 ps for ZnM and to 220 ps for ZnB. Therefore, according to eq 2, the respective injection rate constants are 9.4 × 10^9 s^{-1} (ZnM) and 3.7 × 10^9 s^{-1} (ZnB). Correspondingly, injection quantum yields ($\Phi_{inj} = k_{inj}\tau_{TiO_2}$) of the order of 89% (ZnM) and of 81% (ZnB) were obtained. Thus, both meso disubstituted push−pull and *β*-monosubstituted porphyrinic dyes exhibit similarly high injection quantum yields, more than 80%, with a relative variation of only 8% in favor of the push−pull architecture. These high quantum yields are consistent with the observation of a largely dominant population of oxidized dye generated within the nanosecond laser pulse (see next section).

It is clear that the injection rate constant, evaluated by considering static quenching experiments, represents just an average value, incorporating all the various rate constants originated by the inherent inhomogeneity of the sensitized mesoporous surface. In fact, different dye populations, occupying different adsorption sites, can interact in slightly different ways with the semiconductor and can feel slightly different chemical environments which impact, for example, on the local reorganization energy of the dye and on the electronic coupling with the acceptor states of TiO_2. All these factors have a known influence on the electron transfer kinetics. Previous ultrafast studies of porphyrin-sensitized photoanodes, pointed out that, indeed, although a fraction of dyes injected on ultrafast time scales, an inhomogeneous electron injection behavior was displayed, resulting in the deactivation of a fraction of dye population also in the subnanosecond time scale.[25] This evidence was invoked as a possible photocurrent limiting source in DSSC based on porphyrinic dyes.

It is also evident, as pointed out by TCSPC results, that the residual emission observed on TiO_2 electrode bears also the contribution by dye molecules which are substantially decoupled from the semiconductor surface, following deactivation pathways analogous to those observed on inert ZrO_2 and for which k_{inj} is essentially 0. As a result, it is clear that the average injection rate constants, herein reported, represent a lower limit to the true charge injection rate on TiO_2. However, when k_{inj} is multiplied by τ_{TiO2} to yield Φ_{inj}, the underestimation on the injection rate constant is compensated by an overestimation of the excited state lifetime on TiO_2 surfaces, leading to some cancellation of errors. Thus, the Φ_{inj} values should represent quantitatively useful parameters for evaluating the average performance of the sensitizers, in chemical conditions similar to those experienced in the working solar devices. Hence, in combination with other efficiency figures, the injection quantum yield can be reasonably exploited to predict the maximum IPCE which can be generated by these dyes, as will be later discussed in detail.

Nanosecond Spectroscopy and Dye Regeneration Kinetics. Upon 532 nm excitation of examined porphyrinic dyes in solution, the lowest triplet state (T_1) is populated within the laser pulse (FWHM ≈ 7 ns), setting a $k_{ISC} \geq 1.4 \times 10^8$ s^{-1}. The triplet lifetimes, obtained by monoexponential fitting, are, in aerated conditions, 270 and 560 ns for ZnM and ZnB respectively. In both cases, the differential transient absorption (TA) spectra (Figure 3) are dominated by the intense bleaching of the B band, which results in negative Δ*A* in correspondence of the $S_0 \rightarrow S_2$ absorption of the ground state. In the case of ZnM, at longer wavelength the $T_1 \rightarrow T_n$ absorption dominates, resulting in a broad feature in the 500−610 nm region, followed by the bleaching of the Q bands, spanning the 630−710 nm interval. In the case of ZnB, the bleaching of the B band is followed by an intense triplet−triplet absorption, in the 490−580 nm region, followed by the bleaching of the Q-band, mirroring the ground state absorption, which interrupts an otherwise flat, featureless and relatively weak absorption extending up to 850 nm.

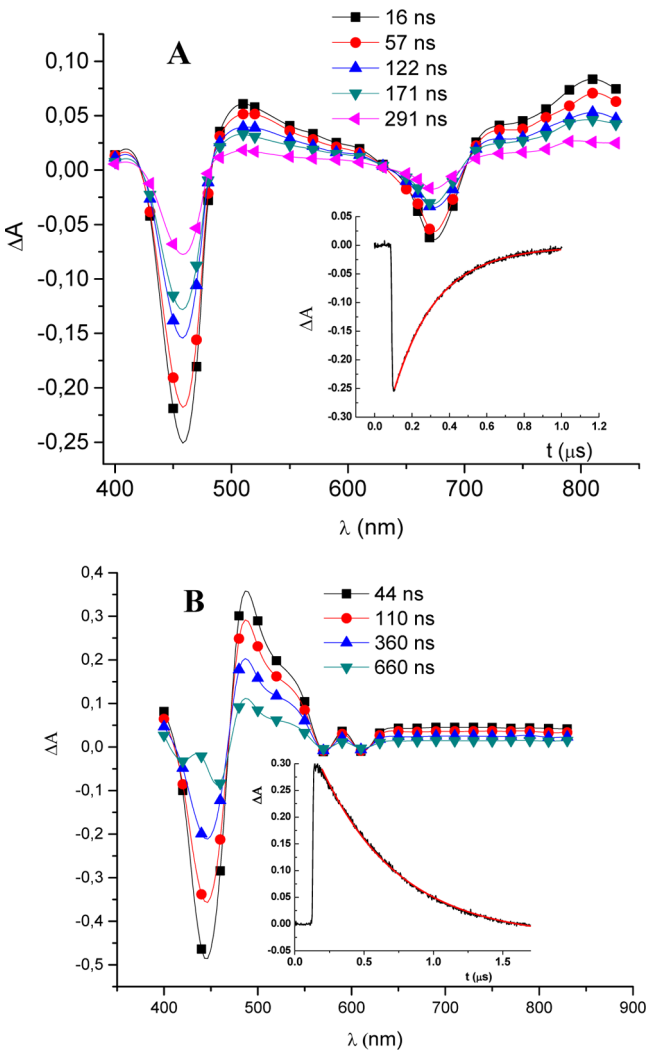

Figure 3. TA spectra of (A) ZnM and (B) ZnB in EtOH/THF solution. Spectra recorded at various time delays after the 532 nm laser excitation are represented. Single wavelength (450 and 500 nm) decays fitted with a monoexponential function are depicted as insets.

The transient difference spectra obtained by 532 nm laser excitation of ZnB and ZnM supported on ZrO_2 thin films are consistent with the formation of their triplet state exhibiting in both cases a lifetime of ca. 350 ns. The triplet state signature of ZnB (see Figure S4A in the Supporting Information) is dominated by the intense absorption band having a relatively sharp maximum in the 500−520 nm interval, as previously

observed in solution, followed by the bleaching of the Q bands. The bleaching of the Soret band could only be partly explored (λ > 440 nm), and its weak intensity relative to the 500 nm absorption is motivated by the excessive optical density (OD >2.5) in this spectral interval. Such strong absorption was determined by the need of reaching a sufficient light harvesting for the 532 nm excitation, a wavelength where the extinction coefficient of the porphyrin is poor. On the other hand, ZnM (see Figure S4C in the Supporting Information), whose absorption spectrum is generally red-shifted with respect to ZnB, is characterized by the intense Soret bleaching centered at 450 nm and by a relatively broad and intense absorption peaking at 550 nm, followed by the weaker but clear Q-band bleaching. The agreement with the TA recorded in fluid solution is excellent. For both dyes, due to the strong light scattering of ZrO_2 films, an intense emission was observed in the red region of the visible spectrum, at very short delays (few ns) after the peak of the laser pulse, consistent with the deactivation of their lowest singlet excited state. The transient emission spectra (see Figure S4B, D in the Supporting Information) agree very well with those observed in both solution and on similar solid substrates by steady-state techniques.

In the case of dyes adsorbed on TiO_2 film (Figure 4), it is at first glance evident that the TA spectra do not show significant resemblance nor contributions from the triplet state, indicating that the charge separated state, consisting of dye cation and electron injected in the conduction band of the semiconductor ($dye^+/e^-(CB)$), is formed in prevailing proportions (at least >80%) within the laser pulse. Hence, the charge injection is dominating over other photophysical deactivation pathways of the excited state. This is consistent with the large charge injection quantum yields estimated in the previous section, although in that case the S_2 excited state was directly populated upon excitation of the B band at 460 nm. Herein, since at 532 nm a quite undefined absorption manifold of the dye, between the B and Q-band is intercepted, the laser excitation should prevailingly populate the S_1 state from which charge injection also occurs with large yields. Thus, it is not clear whether charge injection occurs from S_2, S_1, or both. IPCE spectra previously recorded for similar porphyrinic dyes, when the light harvesting efficiency was unitary for both B and Q bands, suggested that at least a fraction of injection could occur directly from the S_2 excited states.[14,17]

The TA spectra of the two dyes adsorbed onto TiO_2 film (Figure 4) show common features that are ascribed to the spectral characteristics of the radical cation formed by charge injection. The bleaching of the B band (shown from 450 nm) is followed by a weak absorption, which anticipates the deep bleaching of the Q bands (respectively at 630−700 nm for ZnM, and at 530−630 nm for ZnB) and by an intense, triangular shaped absorption band at longer wavelengths. In the absence of electrolyte as electron donor, the recovery of the charge separated state occurs by electron recapture from conduction band by the dye cation ($(e^-)CB + dye^+ \rightarrow dye$). Taking into account that electron recombination occurs from a distribution of energetically different states on the sensitized surface, the kinetics is preferably described by multiexponential functions. In our case a biexponential function afforded good results, with an average lifetime calculated according to eq 6[29]

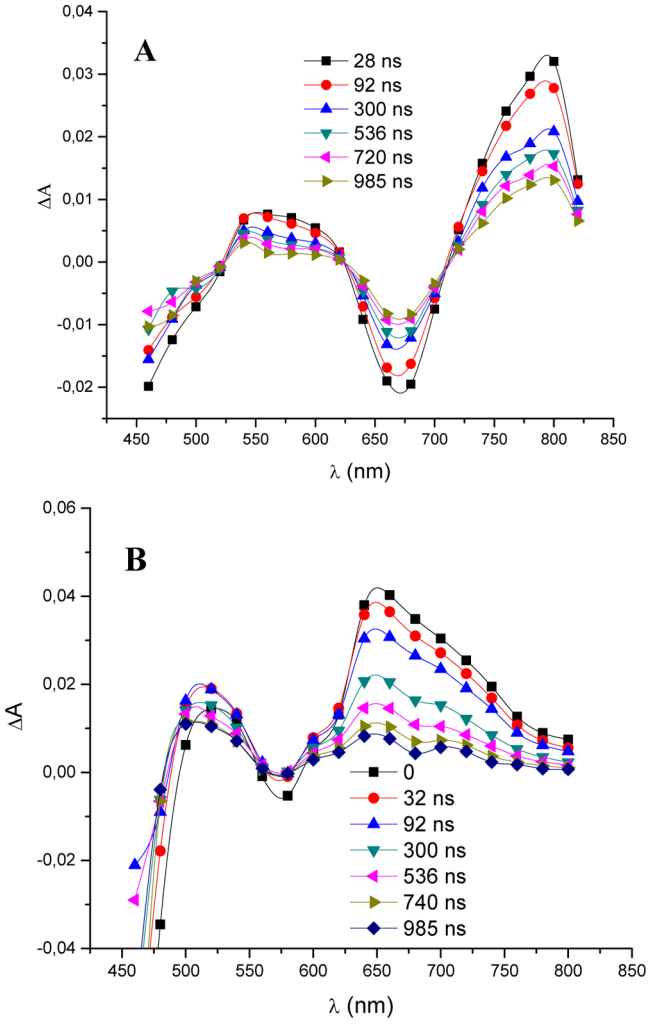

Figure 4. Time evolution of TA spectra of (A) ZnM and (B) ZnB loaded onto TiO_2 thin films in contact with 0.1 M $LiClO_4$ in CH_3CN.

$$\langle\tau\rangle = \sum_i \frac{A_i\tau_i^2}{A_i\tau_i} \quad (6)$$

where A_1 and A_2 and τ_1 and τ_2 are the amplitudes and the lifetimes of the fitting function

$$y = A_1\exp(-t/\tau_1) + A_2\exp(-t/\tau_2) + y_0 \quad (7)$$

In both cases, the dye cations did not recover completely on a time scale of 2 μs and $\langle\tau\rangle$ values equal to 800 ns and 680 ns were obtained for ZnM and ZnB cations, respectively. The longer lifetime of the ZnM cation may be a consequence of hole localization on the amino group farthest from the TiO_2 surface.

The recovery of both dye cations, monitored at 680 nm, employing various laser excitation energies in the presence of electron donating electrolyte (0.6 M AMII + 0.1 M LiI) is reported in Figure 5A, C. It is noteworthy that in all cases, the recovery is considerably accelerated due to electron transfer by I^- and was 90% complete within about 1 μs. The regeneration efficiency term η, which would correspond to the electron collection efficiency, if losses due to recombination with the oxidized electron mediator (I_3^-) were negligible, can be expressed by means of pseudo-first order rate constants. Thus, η is obtained by the reciprocal of either the average

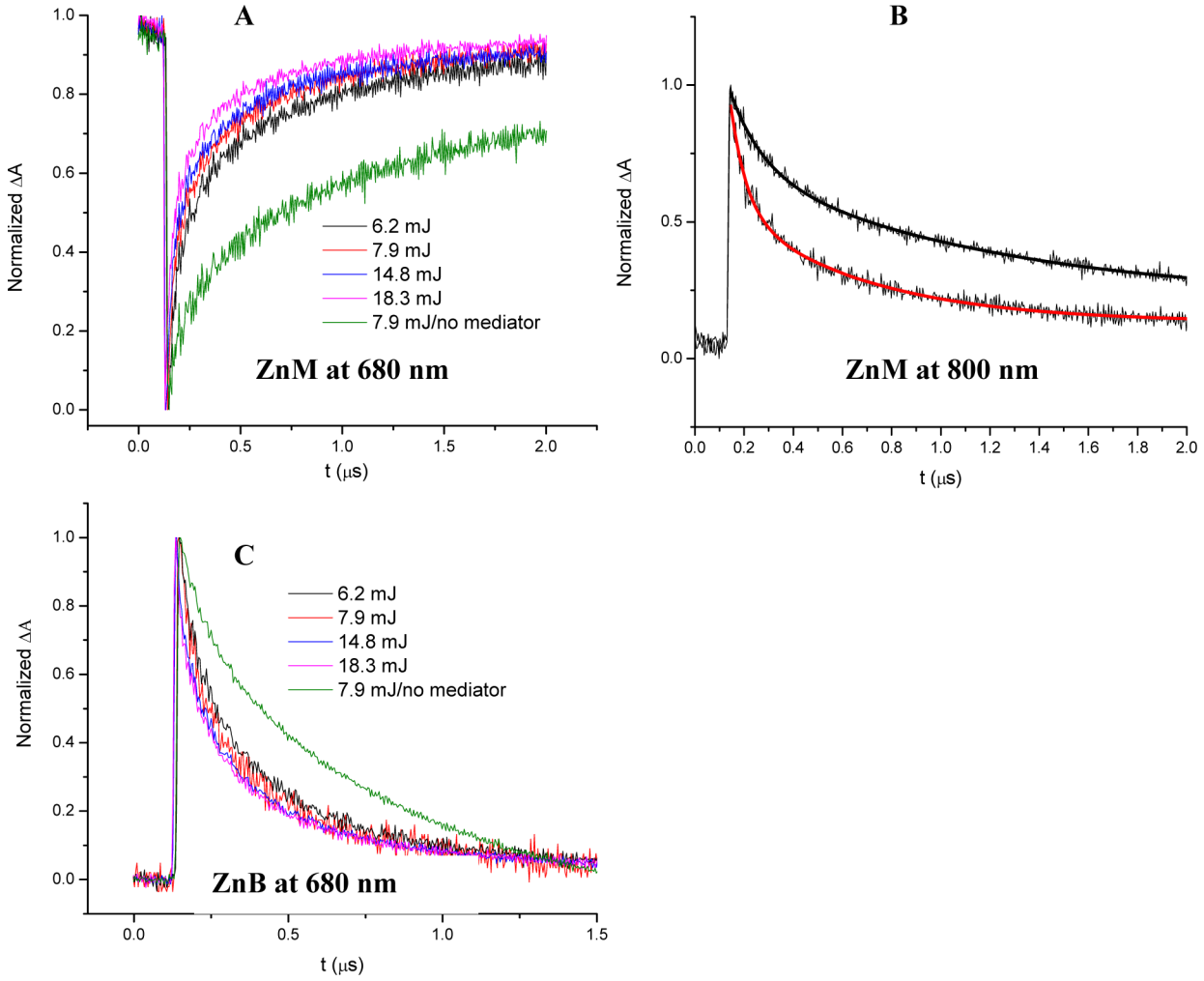

Figure 5. Dye cation recovery in the presence of I^-. (A) ZnM at 680 nm; (B) ZnM at 800 nm in the presence (red) and in the absence (black) of I^-. Excitation energy 7.9 mJ/pulse/cm^2. (C) ZnB at 680 nm. In A–C, various laser excitation energies (mJ/pulse/cm^2) were employed in order to investigate the dependence of the dye recovery from the excitation energy in the presence of electrolyte containing electron donating I^-.

lifetime or the half-life $\tau_{1/2}$ (the time at which 50% of the initial amplitude is decayed) according to the eqs 7 and 8

$$\eta = \frac{\frac{1}{\langle\tau_{reg}\rangle}}{\frac{1}{\langle\tau_{reg}\rangle} + \frac{1}{\langle\tau_{rec}\rangle}} \quad (7)$$

or

$$\eta = \frac{\frac{1}{\langle\tau_{1/2reg}\rangle}}{\frac{1}{\langle\tau_{1/2reg}\rangle} + \frac{1}{\langle\tau_{1/2rec}\rangle}} \quad (8)$$

where $\langle\tau_{reg}\rangle$ is the average regeneration lifetime calculated according to eq 6 in the presence of electron donating species (I^-) and $\langle\tau_{rec}\rangle$ is the average recombination lifetime measured by working in the presence of inert $LiClO_4$ solution.

Typical experiments were conducted with an excitation energy of 7.9 mJ/cm^2/pulse corresponding to a laser pumping at 1.3 kV. Under these conditions, the regeneration efficiency (η) calculated for ZnB working at 680 nm was 75 ± 1% by using either $\tau_{1/2}$ or $\langle\tau\rangle$. For ZnM the regeneration efficiency, calculated at 680 nm (bleaching), resulted in 85 or 78% by using $\tau_{1/2}$ and $\langle\tau\rangle$, respectively. Furthermore, in the case of ZnM, the dye cation recovery was also followed at 800 nm (absorption) with an excitation energy of 7.9 mJ cm^{-2} pulse^{-1} (Figure 5B). At this latter wavelength η = 77% calculated by $\tau_{1/2}$ or 73% by $\langle\tau\rangle$, showing a good agreement with the kinetics followed at 680 nm, confirming that in ZnM both the bleaching and the intense long wavelength absorption were spectral signatures of ZnM^+, following the same kinetic regime with a very good approximation. However, the kinetics monitored at 800 nm resulted in a slightly lower regeneration term and a longer average lifetime (960 ns) with respect to those calculated at 680 nm. These results are probably ascribed to the positive optical contribution of photoinjected electrons trapped in long-lived surface states which are obviously insensitive to the presence of electron donating species, leading to the incomplete TA recovery at 800 nm (Figure 5B, red line), despite of the presence of I^-.

It must be pointed out that in order to extract signals with a good signal-to-noise ratio, we used excitation energies higher than 6.2 mJ/cm^2/pulse in these experiments. Under these conditions, more than 100 electrons per particle are injected by each laser pulse, significantly accelerating recombination with respect to common solar illumination conditions, where few electrons/particle are produced. Indeed the increase in excitation pulse energy, generally causes an acceleration of the dye recovery, because of accelerated recombination

resulting from the increasingly larger number of electrons that populate each nanoparticle. Nevertheless, a triplication in pulse energy (Figure 5A, C) had an overall minor impact in the acceleration of the dye recovery (particularly in the case of ZnB) indicating that even under relatively high pulse energies, regeneration dominates over recombination, allowing to extract reasonable η terms, in spite of the fact that the two competing processes were not completely decoupled.

The above-reported measurements confirm that both dyes are effectively regenerated by the electron mediator I^-, resulting in regeneration efficiencies of the order of 74% for ZnB and close to 80% for ZnM. In principle the regeneration term can be used as a first estimate of the electron collection efficiency (η) when electron losses by recombination with I_3^- are neglected. This is a reasonable assumption under short circuit conditions and low intensity monochromatic illumination, the condition under which IPCE is usually measured, resulting in a lower stationary electron density on the TiO_2 photoanode. Because IPCE = Φ_{inj} η LHE, by considering spectral regions where the light harvesting efficiency (LHE) is unitary, and using the previously evaluated Φ_{inj} and η terms, an extrapolated maximum IPCE = (85 ± 4)% × (75 ± 2)% = (64 ± 4)% was obtained for both dyes, even by making the most conservative hypothesis about the η values. We can thus conclude that the calculated values are in good agreement with recently published experimental results,[17] where the maximum IPCEs for a series of β substituted and meso substituted dyes ranged from 60 to 70%. This is remarkable if we consider that the former were based on the estimation of the efficiencies of the elementary interfacial processes in half cells (photoanodes) under open circuit and in illumination conditions different than those experienced by a DSSC device under either natural or simulated sunlight.

Photoelectrochemical Investigation. In the DSSC, the solar energy conversion efficiency is influenced both by the intrinsic structural and electronic properties of the dye and by a variety of extrinsic factors, including primarily the quality, the thickness and the particle size of TiO_2, the adsorption conditions and the composition of the electrolyte.

In the attempt to optimize the solar cell fabrication parameters, acting on the extrinsic factors, some differences were obtained in photovoltaic performances with respect to those previously reported for the same dyes,[17] although the general trend remained unaffected.

The significant efficiency figures, obtained in DSSCs sensitized with ZnM and ZnB measured under AM 1.5 G illumination are listed in Table 2.

Table 2. Photovoltaic Characteristics of DSSCs Based on ZnB and ZnM Dyes: Short Circuit Photocurrent (J_{sc}), Open Circuit Photovoltage (V_{oc}), Fill Factor (FF), and Power Conversion Efficiency (PCE)

dye	J_{sc} (mA cm^{-2})	V_{oc} (mV)	FF	PCE (%)
ZnB	11.7	675	0.77	6.1
ZnM	8.6	612	0.75	3.9

The PCE of devices based on ZnB and ZnM dyes were 6.1%, and 3.9%, respectively. The greater efficiency of ZnB is evidently due to a general improvement of all photovoltaic parameters with respect to those of ZnM: J_{sc} is increased from 8.6 mA cm^{-2} (ZnM) to 11.7 mA cm^{-2} (ZnB) and V_{oc} is increased by ca. 10% and also the Fill Factor undergoes a 2.6% enhancement.

Because the quantum yield of charge injection and the regeneration efficiency of the two dyes were found to be quite similar, it is likely that the observed differences in the solar energy conversion efficiencies may be ascribed to significant differences in electronic recapture kinetics by the oxidized electrolyte, a process which is usually not easily evaluated by photophysical investigations.

The JV curves of DSSC devices based on ZnM and ZnB are reported in Figure 6 both under illumination and in dark

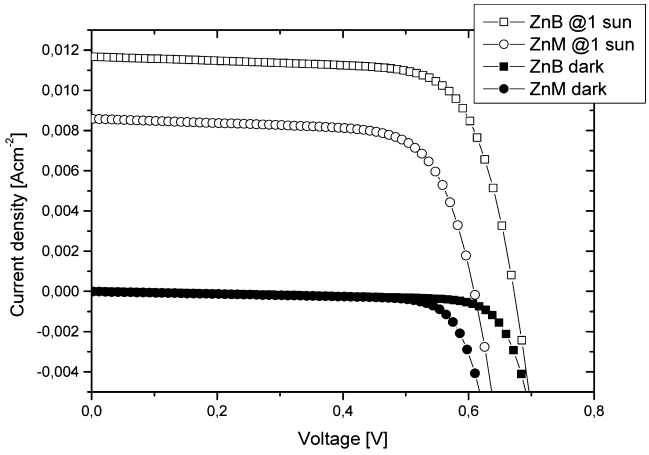

Figure 6. Current−voltage characteristics of DSSCs using dyes ZnB and ZnM under illumination and in dark conditions.

conditions. It is noteworthy that the dark current of ZnM exhibits an anticipated (by ca. 100 mV) onset with respect to that of ZnB (Figure 6 black symbols), providing a strong indication of a more facile I_3^- reduction kinetics at the surface of the TiO_2 photoanode sensitized by the meso push−pull Zn^{II}-porphyrinate. Interestingly, these findings may rationally explain the trend of performances of analogous dyes, previously reported[17] using a different electrolyte, featuring better photovoltaic characteristics by a β pyrrolic substituted tetraarylporphyrinic architecture compared to a meso disubstituted push−pull diarylporphyrinic geometry.

Electrochemical impedance spectroscopy (EIS) investigation has allowed us to corroborate the indications obtained by the $J-V$ curves. The impedance of a DSSC device is modeled with an equivalent electric circuit, in which the electrical elements represent the different cell processes and their interfaces.[30] The charge transfer resistance at the TiO_2/dye/electrolyte interface, R_{ct} (Figure 7A), and the measured capacitance, C_{meas} (Figure 7B), provide quantitative information about the dynamics of electron recapture by I_3^- at the interface of TiO_2 sensitized with either ZnM or ZnB.

C_{meas} and R_{ct} values are plotted as a function of the potential corrected by the IR drop. At intermediate and high potentials, the dominating capacitance is the chemical capacitance C_μ of TiO_2, which shows a characteristic exponential variation with the potential. It is clear that the recombination process significantly affects the apparent electron lifetime on the TiO_2 photoanode, which can be calculated by the equation

$$\tau = R_{ct}C_\mu \quad (9)$$

ZnB exhibits a higher value of capacitance and in particular higher charge transfer resistance resulting in a longer apparent

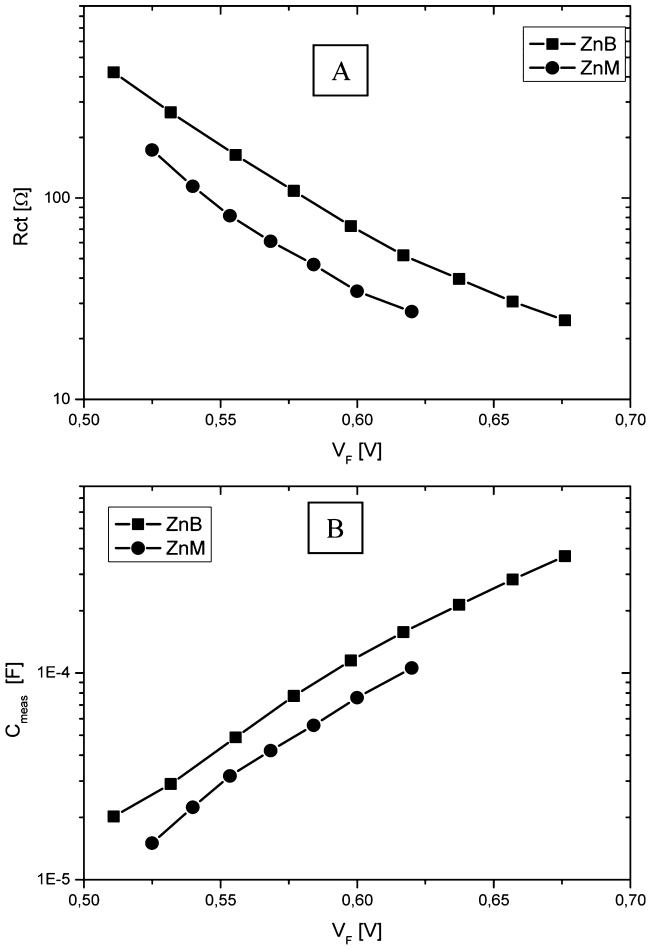

Figure 7. (A) Charge transfer resistance R_{ct} and (B) measured capacitance C_{meas} as functions of the corrected potential for ZnB and ZnM sensitized solar cells under illumination.

electron lifetime (Figure 8) with respect to ZnM. Such results appear to confirm that the recombination process between electrons injected into the TiO_2 film and the oxidized species in the electrolyte (I_3^-) is less critical for the 2-β-substituted porphyrinic dye, ZnB, leading to the enhanced photovoltaic efficiencies, as reported in Table 2.

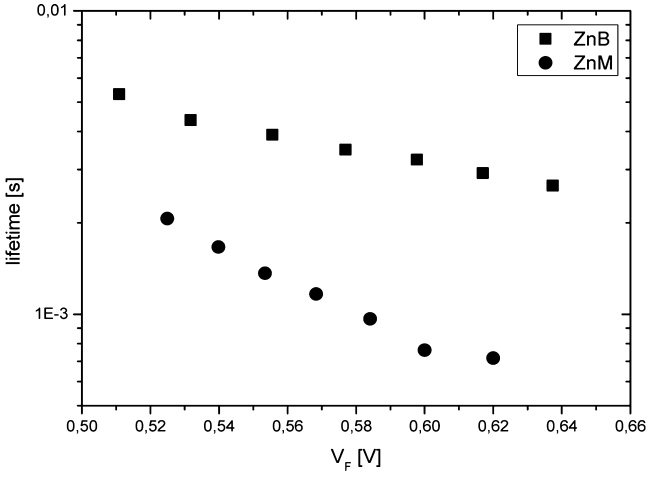

Figure 8. Apparent electron lifetimes as a function of the corrected potential for the ZnB- and ZnM-based DSSCs under illumination.

Significant differences in the dye adsorption of ZnB and ZnM onto TiO_2 can influence recombination kinetics, because TiO_2 sites left uncovered by the dye and exposed to the electrolyte may become preferential recombination centers. However, the spectrophotometric evaluation (see Figure S5 in the Supporting Information) of the dye coverage on transparent thin TiO_2 layers, after 2 h of adsorption in conditions identical to those adopted for the DSSCs fabrication, led to essentially identical surface concentration of the two dyes ($\Gamma = 1.6 \times 10^{-8}$ mol/cm^2). If this result is extended to DSSCs, we can rule out any significant contribution arising from the different surface concentration to the slower recombination kinetics observed for ZnB compared to ZnM. Hence, intrinsic differences in the molecular structure of the two dyes, could play a key role in the passivation of the TiO_2 surface by interaction with I_3^-. In agreement with the latter hypothesis, the higher steric hindrance of ZnB, based on a tridimensional tetraarylporphyrinic core, with respect to ZnM, consisting of a pseudoplanar diaryl porphyrinic core, should play a relevant role. The bulky architecture of the β-substituted porphyrinic dye, as ZnB, should be able to better screen the surface against the approaching oxidized species of the electrolyte compared to a diaryl-porphyrinic dye arranged in a meso push−pull system, as ZnM, thus reducing the recombination rate between the electron accepting I_3^- and the electrons injected on TiO_2. Space filling models of free ZnB and ZnM (see Figure S6 in the Supporting Information) confirm a more bulky structure of 2-β substituted tetraarylporphyrin ZnB with respect to the 5,15-meso disubstituted diarylporphyrin ZnM. Moreover the improved shielding effect of ZnB, which consequently results in a better passivation of the photoanode, can be visualized with relative ease from the top and side views (under the same perspective) of an idealized (101) titania surface (projected area 11 × 18 Å^2) (see Figure S6 in the Supporting Information), bearing two molecules of either ZnM or ZnB arbitrarily bound to titanium centers on the surface.

Furthermore, one of the major aspects that may reduce photovoltaic performances of metal porphyrins when used as dye in DSSC is the formation of aggregates on the semiconductor surface. These are critical aspects in the case of meso disubstituted Zn^{II} porphyrinates, as previously confirmed by the evidence that the introduction of long alkoxy chains on the aryl rings, instead of the more common *tert*-butyl groups, can sterically protect the porphyrinic core retarding the charge recombination process and, in parallel, effectively reduce the dye aggregation, thus allowing for a more efficient electron injection.[3,5]

A second hypothetic mechanism, which may favor recombination processes in the case of meso push−pull architectures, is a local increase of I_3^- concentration due to the formation of charge transfer adducts with the push-amino group. This can favor the approach between I_3^- and the TiO_2 or, in addition, it can result in the oxidative quenching of the dye excited state by charge transfer to the electrolyte. This latter possibility for increased recombination rates and excited state deactivation has been reported for some coordination compounds bearing π-delocalized ligands[31,32] and for macrocyclic aromatic compound such as phtalocyanines[33] and it is currently under investigation in our laboratories. Hence the lack of the amino-group could also contribute to make the ZnB dye less sensitive to the oxidative quenching and should further prevent recombination by reducing the local surface concentration of electron accepting species (I_3^- and I_2).

CONCLUSIONS

In this work, we have comparatively investigated, by combining time-resolved spectroscopy, photophysical and photoelectrochemical techniques, two structurally different dyes which exhibit β monosubstituted Zn^{II}-tetraarylporfirinic (ZnB) and meso disubstituted push−pull Zn^{II}-diarylporphyrinic (ZnM) architecture. The purpose was to clarify the origin of different efficiencies registered in DSSCs based on the two porphyrinic dyes by characterizing and comparing the fundamentals of the interfacial charge separation and collection processes occurring at the dye-sensitized TiO_2 photoanode.

Both dyes showed injection quantum yields ≥80% and displayed a favorable kinetic competition between electron recombination and regeneration, yielding regeneration efficiencies in the 75−85% range. These findings were consistent with previous experimental IPCE data, corresponding to maximum monochromatic conversion efficiency ranging between 60 and 70%, measured in iodide/iodine (I^-/I_3^-) mediated DSSCs.

We have also confirmed the rather unexpected evidence that the β-substituted Zn^{II}-tetraaryl-porphyrinate ZnB display, in DSSC, superior solar-energy conversion efficiency (6.1%) than the meso disubstituted push−pull diaryl-porphyrinate ZnM (3.9%) under simulated solar illumination, thanks to a combination of superior J_{sc}, photovoltage, and fill factor. The photophysical investigation, combining steady state quenching experiments and time-resolved techniques, has evidenced quite similar charge injection and regeneration efficiencies for both dyes. Furthermore, identical dye concentrations were measured on transparent thin TiO_2 layers, thus ruling out any possible influence of different loading degrees on the recombination kinetics. The origin of the higher efficiency of DSSCs based on ZnB appears to be ascribed, on the basis of EIS investigation, to an intrinsic superior passivation of the TiO_2 surface against charge recombination involving electron accepting species of the electrolyte. A superior screening effect, as well as reduced π-staking aggregation, are related, as shown by computational modeling, to the higher steric hindrance of the tetraarylporphyrinic architecture of the β-substituted dye, arising from the presence of four bulky *tert*-butyl-substituted aryl rings surrounding the porphyrinic core. Conversely, the *meso* disubstituted push−pull diarylporphyrinic dye ZnM features a lower sterical crowding and the presence of push-amino group which may promote the formation of adducts with I_3^-, favoring either oxidative quenching of the excited state of the dye or recombination processes with the electrons of the photoanode, because of an increased local surface excess of I_3^-. Hence, we can conclude that the better performance of DSSCs based on ZnB with respect to ZnM, reasonably depends on a significant reduction of the recombination rate with the oxidized redox mediator rather than on differences in regeneration efficiency or charge injection yield.

The information extracted from this study will be helpful in guiding the development of new β-substituted porphyrinic dyes being characterized by a relatively straightforward synthesis with good yields and by a significant steric hindrance. Such a class of dyes appears to be a remarkable, viable, and efficient alternative to more synthetically demanding diarylporphyrinic dyes exhibiting the push−pull meso geometry. Finally, our findings appear to disprove the "paradigm", whereby, up to now, the meso disubstituted push−pull diarylporphyrinic dyes were considered to have the best performing architecture, at least in the case of iodide-iodine mediated DSSCs.

ASSOCIATED CONTENT

Supporting Information

Emission spectra on ZrO_2 thin films (Figure S1), integrated emission spectra of ZnM and ZnB on ZrO_2 and TiO_2, and emission decays measured by TCSPC (Figure S3). Transient absorption and emission spectra on ZrO_2 thin films (Figure S4), and absorption spectra (Figure S5) and computational models of dyes ZnB and ZnM (Figure S6). This material is available free of charge via the Internet at http://pubs.acs.org.

AUTHOR INFORMATION

Corresponding Authors

*E-mail: gabriele.dicarlo@unimi.it.
*E-mail: cte@unife.it.

Notes

The authors declare no competing financial interest.

ACKNOWLEDGMENTS

G.D.C, A.O.B., F.T., and M.P. thank Prof. Renato Ugo for the fundamental advices and the useful discussions. V.T., R.G., and L.D.M. are grateful to the national research project for financial support MAAT (MAAT (MIUR- PON02_00563_3316357 − CUP B31C12001230005)). PRIN 2011 (Unife) is gratefully acknowledged for funding.

REFERENCES

(1) Mussini, P. R.; Orbelli Biroli, A.; Tessore, F.; Pizzotti, M.; Biaggi, C.; Di Carlo, G.; Lobello, M. G.; De Angelis, F. Modulating the Electronic Properties of Asymmetric Push−Pull and Symmetric Zn(II)-Diarylporphyrinates with Para Substituted Phenylethynyl Moieties in 5,15 Meso Positions: A Combined Electrochemical and Spectroscopic Investigation. *Electrochim. Acta* **2012**, *85*, 509−523.

(2) Lo, C.-F.; Hsu, S.-J.; Wang, C.-L.; Cheng, Y.-H.; Lu, H.-P.; Diau, E. W.-G.; Lin, C.-Y. Tuning Spectral and Electrochemical Properties of Porphyrin-Sensitized Solar Cells. *J. Phys. Chem. C* **2010**, *114*, 12018−12023.

(3) Li, L.-L.; Diau, E. W.-G. Porphyrin-Sensitized Solar Cells. *Chem. Soc. Rev.* **2013**, *42*, 291−304.

(4) Bessho, T.; Zakeeruddin, S. M.; Yeh, C.-Y.; Diau, E. W.-G.; Grätzel, M. Highly Efficient Mesoscopic Dye-Sensitized Solar Cells Based on Donor−Acceptor-Substituted Porphyrins. *Angew. Chem., Int. Ed.* **2010**, *49*, 6646−6649.

(5) Chang, Y.-C.; Wang, C.-L.; Pan, T.-Y.; Hong, S.-H.; Lan, C.-M.; Kuo, H.-H.; Lo, C.-F.; Hsu, H.-Y.; Lin, C.-Y.; Diau, E. W.-G. A Strategy to Design Highly Efficient Porphyrin Sensitizers for Dye-Sensitized Solar Cells. *Chem. Commun.* **2011**, *47*, 8910−8912.

(6) Lee, C.-W.; Lu, H.-P.; Lan, C.-M.; Huang, Y.-L.; Liang, Y.-R.; Yen, W.-N.; Liu, Y.-C.; Lin, Y.-S.; Diau, E. W.-G.; Yeh, C.-Y. Novel Zinc Porphyrin Sensitizers for Dye-Sensitized Solar Cells: Synthesis and Spectral, Electrochemical, and Photovoltaic Properties. *Chem.—Eur. J.* **2009**, *15* (6), 1403−1412.

(7) Campbell, W. M.; Jolley, K. W.; Wagner, P.; Wagner, K.; Walsh, P. J.; Gordon, K. C.; Schmidt-Mende, L.; Nazeeruddin, M. K.; Wang, Q.; Grätzel, M.; Officer, D. L. Highly Efficient Porphyrin Sensitizers for Dye-Sensitized Solar Cells. *J. Phys. Chem. C* **2007**, *111*, 11760−11762.

(8) LeCours, S. M.; DiMagno, S. G.; Therien, M. J. Exceptional Electronic Modulation of Porphyrins through Meso-Arylethynyl Groups. Electronic Spectroscopy, Electronic Structure, and Electrochemistry of 5,15-Bis (Aryl)Ethynyl −10,20-Diphenylporphinato Zinc(II) Complexes. X-ray Crystal Structures of 5,15-Bis (4′-Fluorophenyl)Ethynyl −10,20-Diphenylporphinato Zinc(II) and 5,15-Bis (4′-Methoxyphenyl)Ethynyl −10,20-Diphenylporphyrin. *J. Am. Chem. Soc.* **1996**, *118*, 11854−11864.

(9) LeCours, S. M.; Guan, H. W.; DiMagno, S. G.; Wang, C. H.; Therien, M. J. Push-Pull Arylethynyl Porphyrins: New Chromophores

that Exhibit Large Molecular First-Order Hyperpolarizabilities. *J. Am. Chem. Soc.* **1996**, *118*, 1497−1503.
(10) Yella, A.; Lee, H.-W.; Tsao, H. N.; Yi, C.; Chandiran, A. K.; Nazeeruddin, M. K.; Diau, E. W.-G.; Yeh, C.-Y.; Zakeeruddin, S. M.; Grätzel, M. Porphyrin-Sensitized Solar Cells with Cobalt (II/III)−Based Redox Electrolyte Exceed 12% Efficiency. *Science* **2011**, *334*, 629−634.
(11) Yi, C.; Giordano, F.; Cevey-Ha, N.-L.; Tsao, H. N.; Zakeeruddin, S. M.; Grätzel, M. Influence of Structural Variations in Push−Pull Zinc Porphyrins on Photovoltaic Performance of Dye-Sensitized Solar Cells. *ChemSusChem* **2014**, *7*, 1107−1113.
(12) Mathew, S.; Yella, A.; Gao, P.; Humphry-Baker, R.; Curchod, B. F. E.; Ashari-Astani, N.; Tavernelli, I.; Rothlisberger, U.; Nazeeruddin, M. K.; Graetzel, M. Dye-Sensitized Solar Cells with 13% Efficiency Achieved Through the Molecular Engineering of Porphyrin Sensitizers. *Nat. Chem.* **2014**, *6*, 242−247.
(13) Wang, C.-L.; Lan, C.-M.; Hong, S.-H.; Wang, Y.-F.; Pan, T.-Y.; Chang, C.-W.; Kuo, H.-H.; Kuo, M.-Y.; Diau, E. W.-G.; Lin, C.-Y. Enveloping Porphyrins for Efficient Dye-Sensitized Solar Cells. *Energy Environ. Sci.* **2012**, *5*, 6933−6940.
(14) Orbelli Biroli, A.; Tessore, F.; Pizzotti, M.; Biaggi, C.; Ugo, R.; Caramori, S.; Aliprandi, A.; Bignozzi, C. A.; De Angelis, F.; Giorgi, G.; Licandro, E.; Longhi, E. A Multitechnique Physicochemical Investigation of Various Factors Controlling the Photoaction Spectra and of Some Aspects of the Electron Transfer for a Series of Push−Pull Zn(II) Porphyrins Acting as Dyes in DSSCs. *J. Phys. Chem. C* **2011**, *115*, 23170−23182.
(15) Lindsey, J. S.; Wagner, R. W. Investigation of the Synthesis of Ortho-Substituted Tetraphenylporphyrins. *J. Org. Chem.* **1989**, *54*, 828−836.
(16) Senge, M. O. Stirring the Porphyrin Alphabet Soup-Functionalization Reactions for Porphyrins. *Chem. Commun.* **2011**, *47*, 1943−1960.
(17) Di Carlo, G.; Orbelli Biroli, A.; Pizzotti, M.; Tessore, F.; Trifiletti, V.; Ruffo, R.; Abbotto, A.; Amat, A.; De Angelis, F.; Mussini, P. R. Tetraaryl Zn^{II} Porphyrinates Substituted at β-Pyrrolic Positions as Sensitizers in Dye-Sensitized Solar Cells: A Comparison with meso-Disubstituted Push−Pull Zn^{II} Porphyrinates. *Chem.—Eur. J.* **2013**, *19*, 10723−10740.
(18) Hagfeldt, A.; Boschloo, G.; Sun, L.; Kloo, L.; Pettersson, H. Dye-Sensitized Solar Cells. *Chem. Rev.* **2010**, *110*, 6595−6663.
(19) Hagfeldt, A.; Grätzel, M. Molecular Photovoltaics. *Acc. Chem. Res.* **2000**, *33*, 269−277.
(20) Grätzel, M. Dye-Sensitized Solar Cells. *J. Photochem. Photobiol., C* **2003**, *4*, 145−153.
(21) Campbell, W. M.; Burrell, A. K.; Officer, D. L.; Jolley, K. W. Porphyrins as Light Harvesters in the Dye-Sensitised TiO_2 Solar Cell. *Coord. Chem. Rev.* **2004**, *248*, 1363−1379.
(22) Griffith, M. J.; Sunahara, K.; Wagner, P.; Wagner, K.; Wallace, G. G.; Officer, D. L.; Furube, A.; Katoh, R.; Mori, S.; Mozer, A. J. Porphyrins for Dye-Sensitised Solar Cells: New Insights into Efficiency-Determining Electron Transfer Steps. *Chem. Commun.* **2012**, *48*, 4145−4162.
(23) Wang, Q.; Campbell, W. M.; Bonfantani, E. E.; Jolley, K. W.; Officer, D. L.; Walsh, P. J.; Gordon, K.; Humphry-Baker, R.; Nazeeruddin, M. K.; Grätzel, M. Efficient Light Harvesting by Using Green Zn-Porphyrin-Sensitized Nanocrystalline TiO_2 Films. *J. Phys. Chem. B* **2005**, *109*, 15397−15409.
(24) Lind, S. J.; Gordon, K. C.; Gambhir, S.; Officer, D. L. A Spectroscopic and DFT Study of Thiophene-Substituted Metalloporphyrins as Dye-Sensitized Solar Cell Dyes. *Phys. Chem. Chem. Phys.* **2009**, *11*, 5598−5607.
(25) Sunahara, K.; Furube, A.; Katoh, R.; Mori, S.; Griffith, M. J.; Wallace, G. G.; Wagner, P.; Officer, D. L.; Mozer, A. J. Coexistence of Femtosecond- and Nonelectron-Injecting Dyes in Dye-Sensitized Solar Cells: Inhomogeniety Limits the Efficiency. *J. Phys. Chem. C* **2011**, *115*, 22084−22088.
(26) Ning, Z.; Fu, Y.; Tian, H. Improvement of dye-sensitized solar cells: what we know and what we need to know. *Energy Environ. Sci.* **2010**, *3*, 1170−1181.
(27) Magne, C.; Urien, M.; Ciofini, I.; Tugsuz, T.; Pauporte, T. Amphiphilic Acids as Co-Adsorbents of Metal-Free Organic Dyes for the Efficient Sensitization of Nanostructured Photoelectrode. *RSC Adv.* **2012**, *2*, 11836−11842.
(28) Mba, M.; D'Acunzo, M.; Salice, P.; Carofiglio, T.; Maggini, M.; Caramori, S.; Campana, A.; Aliprandi, A.; Argazzi, R.; Carli, S.; Bignozzi, C. A. Sensitization of Nanocrystalline TiO2 with Multi-branched Organic Dyes and Co(III)/(II) Mediators: Strategies to Improve Charge Collection Efficiency. *J. Phys. Chem. C* **2013**, *117*, 19885−19896.
(29) Song, W.; Brennaman, M. K.; Concepcion, J. J.; Jurss, J. W.; Hoertz, P. G.; Luo, H.; Chen, C.; Hanson, K.; Meyer, T. J. Interfacial Electron Transfer Dynamics for [Ru(bpy)2((4,4′-PO3H2)2bpy)]2+ Sensitized TiO2 in a Dye-Sensitized Photoelectrosynthesis Cell: Factors Influencing Efficiency and Dynamics. *J. Phys. Chem. C* **2011**, *115*, 7081−7091.
(30) Bisquert, J.; Fabregat-Santiago, F.; Mora-Seró, I.; Garcia-Belmonte, G.; Giménez, S. Electron Lifetime in Dye-Sensitized Solar Cells: Theory and Interpretation of Measurements. *J. Phys. Chem. C* **2009**, *113*, 17278−17290.
(31) Gardner, J. M.; Abrahamsson, M.; Farnum, B. H.; Meyer, G. J. Visible Light Generation of Iodine Atoms and I−I Bonds: Sensitized I− Oxidation and I3− Photodissociation. *J. Am. Chem. Soc.* **2009**, *131*, 16206−16214.
(32) Rowley, J. G.; Farnum, B. H.; Ardo, S.; Meyer, G. J. Iodide Chemistry in Dye-Sensitized Solar Cells: Making and Breaking I−I Bonds for Solar Energy Conversion. *J. Phys. Chem. Lett.* **2010**, *1*, 3132−3140.
(33) O'Regan, B. C.; López-Duarte, I.; Martínez-Díaz, M. V.; Forneli, A.; Albero, J.; Morandeira, A.; Palomares, E.; Torres, T.; Durrant, J. R. Catalysis of Recombination and Its Limitation on Open Circuit Voltage for Dye Sensitized Photovoltaic Cells Using Phthalocyanine Dyes. *J. Am. Chem. Soc.* **2008**, *130*, 2906−2907.